A study on microstructure and magnetic properties of nanostructured $Co_xNi_{1-x}Mn_{0.5}Fe_{1.5}O_4$($x = 0, 0.25, 0.5, 0.75, 1$) spinel ferrites

A. Hussain[a,*], S. Akbar Tahir[b], N. Ahmad[a], M. Hashim[a], A. Bashir Ziya[c], and S. Noreen[a]

[a] *Department of Physics Khwaja Fareed University of Engineering and Information Technology Rahim Yar Khan-64200, Pakistan.*
[*] *e-mail: abid@kfueit.edu.pk*
[b] *Department of Physics Government College University Faisalabad-38000, Pakistan.*
[c] *Department of Physics Bahauddin Zakariya University Multan-60800, Pakistan.*

Received 10 September 2020; accepted 8 January 2020

A low-temperature synthesis of novel nanostructured $Co_xNi_{1-x}Mn_{0.5}Fe_{1.5}O_4$($x = 0, 0.25, 0.5, 0.75, 1$) ferrites was carried out by sol-gel auto-combustion technique. The obtained nanostructured ferrites were investigated by employing the techniques of powder X-ray diffraction (XRD), scanning electron microscopy (SEM), transmission electron microscopy (TEM), energy dispersive X-ray spectroscopy (EDX), and vibrating sample magnetometry (VSM). The XRD diffractograms of the prepared ferrites revealed the formation of a spinel phase with face-centered cubic (fcc) structure belonging to the Fd-$\bar{3}$m space group. The average lattice parameter 'a' of ferrites exhibited a rise versus a rise in Co^{2+} concentration following Vegard's law. The SEM investigation of $NiMn_{0.5}Fe_{1.5}O_4$ powder revealed the existence of octahedral-shaped morphology of ferrite grains. The TEM investigation of $NiMn_{0.5}Fe_{1.5}O_4$ powder showed nanostructures of ferrite particles with sizes consistent with the crystallite sizes as estimated by Debye-Scherer's formula. An EDX spectrum of $NiMn_{0.5}Fe_{1.5}O_4$ powder confirmed its elemental composition. The M-H hysteresis loops recorded by VSM at room temperature revealed a dependence of coercivity (H_c), maximum magnetization (M_{max}), and retentivity (M_r) on Co^{2+} concentration. The shape dependence of M-H loops on Co^{2+} concentration in compounds enabled their candidature for applications in memory devices and magnetic sensors.

Keywords: Sol-gel technique; spinel structure; X-ray diffraction; scanning electron microscopy; coercivity; remanence.

DOI: https://doi.org/10.31349/RevMexFis.67.527

1. Introduction

Nanostructured spinel ferrites with chemical composition MFe_2O_4 (M=Fe, Co, Ni, Mn, Zn, etc.) have attracted enormous attention from the research community for several decades because of their remarkable electrical and magnetic properties. Spinel ferrites are cost-effective materials that possess smaller H_c, smaller saturation magnetization (M_s), and higher M_r. The unusual magnetic behavior of spinel ferrites diversely associates them with various significant technological applications involving the production of multifunctional appliances such as transformer cores, microwave devices, high-density recording media, gas sensors, ferrofluids, read out heads, treatments of contaminated water, organic dye degradations, bactericides and medical equipment [1]. In nanostructured spinel ferrites, electrical and magnetic properties prove to be a function of composition, cations distribution, particle size, surface coating, and synthesis methodology [2]. The structure of a spinel unit cell is based on an fcc oxygen lattice comprising 64 tetrahedral (A-sites) and 32 octahedral (B-sites) interstitial sites. In a spinel structure, the metal cations can occupy only 8 out of 64 available A-sites and 16 out of 32 available B-sites. A spinel structure can be categorized into normal, mixed, and inverse spinels based on cation distribution over two types of interstitial sites. In a normal spinel, all the 8 divalent cations occupy 8 A-sites, and all the 16 trivalent cations occupy 16 B-sites. In an inverse spinel, all the 8 divalent cations occupy 8 of the filled 16 B-sites, and the 16 trivalent cations occupy the left-over 8 A and 8 B sites. Any other intermediate arrangement of cations in the structure makes the ferrite compound a mixed spinel. Spinel ferrites exhibit ferrimagnetism originated from the interactions of magnetic moments of metal cations with anti-parallel spins located at A and B-sites [3]. An application-driven control on the evolution of microstructure and physical properties of spinel compounds is of utmost importance to tune the electromagnetic properties suitable for numerous potential applications. The ferrite compounds like $NiFe_2O_4$ and $CoFe_2O_4$ are inverse spinels, and their application-driven designs are met by adopting appropriate synthesis methodologies besides tailoring of surface morphology of their nanostructured constituents. The synthesis methods commonly used to prepare nanostructured spinel ferrites comprise the techniques of sol-gel auto-combustion, co-precipitation, sonochemistry reaction, reverse micelles, flow injection, micro-emulsion, electrospray, hydrothermal reaction, microwave combustion, solid-state reaction, and high energy ball milling [4,5]. A sol-gel auto-combustion technique can yield pure phase spinel ferrites at nanoscale under optimal reaction conditions. This technique involves a self-ignited, self-sustained course of combustion, and a ferrite powder is yielded by mixing an aqueous solution of metal salts with a fuel of citric acid in the presence of a catalyst content ammonia solution and ethylene glycol which is an oxidizing agent and a surfactant. The organic materials generated and employed during the sol-gel chemical reaction are

eliminated by elevated temperature treatments and thermal annealing in an oxygen-rich environment [6]. The physical properties of a single-phase ferrite compound synthesized by sol-gel technique can be controlled by reaction parameters like stoichiometry of surfactants, solvents, and metal salts as well as by time and temperature of gel-formation, pH of the reaction, and time and temperature of post-growth annealing. An organic solvent and surfactant in a reaction controls the size and shape-morphology of yielded nanostructured ferrite powder. A complete removal of organic contents from interacting surfaces of nanostructured ferrites is extremely important for optimum display of magnetic parameters like M_s and H_c [7,8].

A size growth is induced by an elevated temperature treatment or a prolonged annealing time yielding the nanostructured ferrite particles with larger sizes. Contrarily, the quantum confinement effects like exchange interactions in nanoparticles are optimized by ensuring lager intact surface area among them. For the sake of optimum soft magnetic behaviour, the nanostructured ferrite particles with smaller sizes can be obtained by a low-temperature sol-gel auto-combustion technique involving a shorter post growth annealing time at lower temperature [9,10]. An incorporation of Co^{2+} cations in $NiMn_{0.5}Fe_{1.5}O_4$ compound can widen its application potential causing an enhanced magneto-crystalline anisotropy, higher magnetization and coercivity. So far, a significant research work has been devoted to synthesize $Co_{0.5}Ni_{0.5}Fe_2O_4$ nanoparticles and their composites [10-12]. There is no published data available on the investigations of nanostructured $Ni_{1-x}Co_xFe_{1.5}Mn_{0.5}O_4$ spinel ferrites synthesized by sol-gel auto-combustion technique. Herein, we report an investigation of microstructure and magnetic properties of nanostructured $Ni_{1-x}Co_xFe_{1.5}Mn_{0.5}O_4(x = 0, 0.25, 0.5, 0.75, 1)$ spinel ferrites synthesized by sol-gel auto-combustion technique involving a lower annealing temperature $\sim 600°C$ for a shorter post growth annealing time of 1 h. It was revealed that the microstructural parameters like average lattice parameter a, the particle size D, the X-ray density D_x and the magnetic parameters like H_c and M_s of the ferrite compounds exhibited a severe dependence on the concentration of Co^{2+} cations in $NiFe_{1.5}Mn_{0.5}O_4$ matrix.

2. Experimental procedures

2.1. Materials and methods

A series of nanostructured $Co_xNi_{1-x}Mn_{0.5}Fe_{1.5}O_4(x = 0, 0.25, 0.5, 0.75, 1)$ spinel compounds was prepared by sol-gel auto-combustion technique. Analytical grade metal salts including cobalt nitrate ($Co(NO_3)_2{\cdot}6H_2O$), nickel nitrate ($Ni(NO_3)_2{\cdot}6H_2O$), iron nitrate ($Fe(NO_3)_3{\cdot}9H_2O$), manganese nitrate $Mn(NO_3)_2$, citric acid ($C_6H_8O_7{\cdot}H_2O$), ethylene glycol ($C_2H_6O_2$) and ammonia solution ($NH_3{\cdot}H_2O$) were obtained from Sigma Aldrich and used without further purification. In the stoichiometric calculations, the molar ratio of citric acid to metal nitrates was kept 2: 1 whereas, the molar ratio of ethylene glycol to metal nitrates was set 1:1. The citric acid was used in the proposed chemical reaction as a fuel and ethylene glycol was employed as a surfactant and oxidizing agent for metal cations whereas, the ammonia solution was used as a catalyst. A general synthesis methodology involved the dissolution of corresponding stoichiometric ratios of all the metal nitrates, citric acid, and ethylene glycol in deionized water. The pH of the solution of metal nitrates and organic compounds was adjusted to a neutral value 7 by a dropwise addition of ammonia solution. Later on, the mixed solution was vigorously stirred and heated on a hot plate at a temperature of 80°C. The process of heating and stirring of the mixed solution was continued maintaining a pH$\sim$ 7 until a wet gel was obtained. The removal of water and organic materials from the wet gel was carried out by drying it in an oven at gradually increasing temperature in the presence of air to yield a fluffy powder by self-ignited and self-propagated combustion approach. Later on, the powder product was kept in the oven at a constant temperature of 120°C for 2 h for calcination purposes to obtain a loose spinel ferrite powder. The calcined ferrite powder was ground by agate mortar for 10 min for better homogeneity, and the ground powder was annealed at 600°C for 1 h in a muffle furnace for better crystallinity in the obtained ferrite compounds.

2.2. Characterization

The obtained $Co_xNi_{1-x}Mn_{0.5}Fe_{1.5}O_4$ ferrite compounds were characterized by powder XRD, SEM, EDX, TEM, HRTEM, SAED, and VSM. An investigation of phase formation of the nanostructured compounds was carried out by recording XRD diffractograms using a Siemens Bruker D-5000 diffractometer equipped with Cu-Kα radiation in an angle range $2\theta = 20 - 80°$ operated at 40 kV and 30 mA with a measurement step 0.02°/sec. The XRD diffractograms of all the nanostructured compounds were analyzed to investigate the phase formation and microstructure of the compounds in addition to a Rietveld structural refinement using MDI Jade 6.5 computer software with JCPDS database. A crystallite size D for each spinel compound was estimated using the XRD data of the strongest reflection peak (311) in each pattern employing Debye-Scherer's formula expressed as under:

$$D = \frac{0.9\lambda}{\beta \cos\theta}. \tag{1}$$

For Cu-Kα radiation, the wavelength λ was 1.5406 Å, 2θ was the position of the maximum of a diffraction peak measured in degrees whereas, β was the full width at half maximum of the peak measured in radian. The lattice parameter a of the fcc unit cell of $Co_xNi_{1-x}Mn_{0.5}Fe_{1.5}O_4$ compounds was calculated using an expression described as under:

$$a = \frac{\lambda}{2\sin\theta}\sqrt{h^2 + k^2 + l^2}. \tag{2}$$

Here, h, k, l represented the Miller indices corresponding to the planes causing reflections of notable intensity.

The shape-morphology of $Co_xNi_{1-x}Mn_{0.5}Fe_{1.5}O_4$ powder compound and size of the powder agglomerates was investigated employing a JEOL JSM-6490 SEM operated at 25 kV equipped with an energy dispersive X-ray detector (EDX). An EDX detector was employed to confirm the elemental composition of the $Co_xNi_{1-x}Mn_{0.5}Fe_{1.5}O_4$ ferrite compound. A JEOL JEM-2010F TEM with an accelerating voltage of 200 kV was employed to record a bright-field TEM micrograph, a high-resolution TEM (HRTEM) micrograph, and a selected area electron diffraction (SAED) pattern of nanostructured $Co_xNi_{1-x}Mn_{0.5}Fe_{1.5}O_4$ compound, which were investigated to study the morphology, crystallite size and microstructural details of the compound. Magnetic measurements of the nanostructured $Ni_{1-x}Co_xMn_{0.5}Fe_{1.5}O_4$ compounds were carried out by recording the M-H hysteresis loops at room temperature under a maximum applied field of 15 kOe using a Lakeshore-735 VSM.

3. Results and discussions

3.1. XRD analysis

Figure 1 shows the powder XRD patterns of annealed series of $Co_xNi_{1-x}Mn_{0.5}Fe_{1.5}O_4 (x = 0, 0.25, 0.5, 0.75, 1)$ nanostructured compounds. The XRD patterns were indexed by matching each pattern with the standard patterns of $NiFe_2O_4$ (PDF#74-2081) and $CoFe_2O_4$ (PDF#22-1086) using MDI Jade 6.5 software. It was found that the recorded patterns of the series of compounds were consistent with the standard patterns, and indexing of the recorded patterns led to the

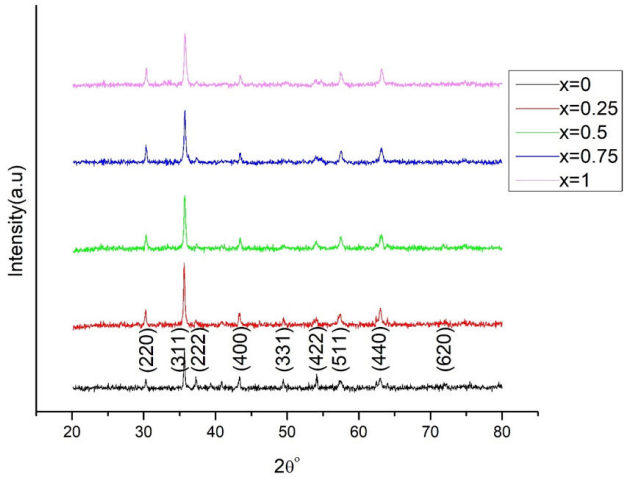

FIGURE 1. Powder X-ray diffraction patterns of $Co_xNi_{1-x}Mn_{0.5}Fe_{1.5}O_4$ ($x = 0, 0.25, 0.5, 0.75, 1$) spinel ferrites.

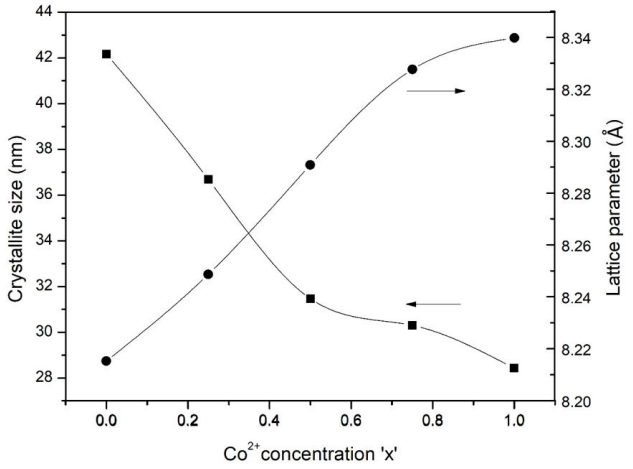

FIGURE 2. A plot of crystallite size D and average lattice parameter a versus Co^{2+} concentration x in $Co_xNi_{1-x}Mn_{0.5}Fe_{1.5}O_4$ spinel ferrites.

Miller indices corresponding to the diffracting planes (220), (311), (222), (400), (331), (422), (511), (440) and (620) of an fcc spinel structure belonging to an Fd-$\bar{3}$m space group.

It was found that no impurity peak was evident in the recorded patterns, which indicated that the prepared ferrite compounds were purely single-phase solid solutions [13]. A gradual broadening of the strongest diffraction peak (311) in the series of recorded patterns merely indicated that the structural parameters like crystallite size D and lattice parameter a of the obtained compounds were a function of composition. It was noted that the ferrite samples with increasing Co^{2+} concentration showed a steady decline in crystallite size D. The crystallite size was estimated by Debye-Scherer's formula using the XRD data of the strongest peak (311) in each XRD pattern which led to a crystallite size range $D \approx 28-42$ nm for obtained $Co_xNi_{1-x}Mn_{0.5}Fe_{1.5}O_4$ compounds [14]. An evolution of the crystallite size D as a function of composition for $Co_xNi_{1-x}Mn_{0.5}Fe_{1.5}O_4$ compounds is shown in Fig. 2. The interplanar spacing d for each peak of the pattern was measured using the formula: $2d\sin\theta = n\lambda$. The lattice parameter for each compound was calculated by employing the formula aforementioned in Eq. (2), which was based on the corresponding data of the XRD patterns. For the sake of accuracy, firstly, the lattice parameter for each peak of the XRD pattern was calculated, and then an average value was deduced, which showed a good agreement with the results reported earlier [15]. It was observed that the average lattice parameter a increased with an increase in the Co^{2+} concentration in the ferrite compounds, which was ascribed to the larger cationic radius (0.74 Å) of Co^{2+} ions compared to that (0.69 Å) of Ni^{2+} ions. A substitution of larger Co^{2+} ions for the smaller host Ni^{2+} ions in the spinel structure caused a shift in the XRD peaks to lower 2θ values, and thus, the average lattice parameter a was increased [16-18]. A variation in the average lattice parameter a with varying Co^{2+} concentration in ferrite compounds fulfilled the conditions of Vegard's law as shown in Fig. 2 [19]. The X-ray density D_x of all the

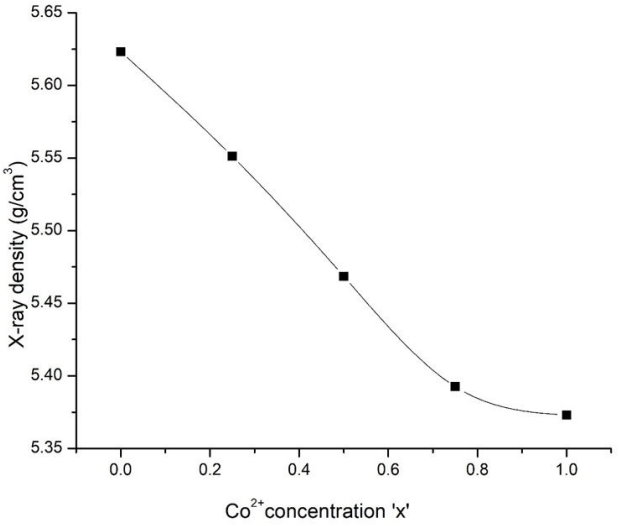

FIGURE 3. A plot of X-ray density D_x versus Co^{2+} concentration x in $Co_xNi_{1-x}Mn_{0.5}Fe_{1.5}O_4$ spinel ferrites.

obtained $Co_xNi_{1-x}Mn_{0.5}Fe_{1.5}O_4$ compounds was determined using a relation $D_x = nM/a^3NA$, where n represented the number of formula units in a spinel unit cell, M represented the molecular weight of a composition, a denoted the average lattice parameter, and 'NA' represented the Avogadro's number (6.0225×1023 atom/mol). A deviation in X-ray density D_x with varying Co^{2+} concentrations in the compounds is depicted in Fig. 3. It was evident that as the Co^{2+} concentration increased, the lattice expansions took place, linking to a gradual rise in the value of the average lattice parameter a contrarily. It was also associated with a decline in crystallite size D [20]. It was revealed that the X-ray density D_x of the ferrite compounds decreased with an increase in the Co^{2+} concentration that was ascribed to the substitution of the larger Co^{2+} cations. On the other hand, the substitution of larger Co^{2+} cations in the compounds resulted in reduced compactness of the crystallites on the behest of lattice expansions inducing a boost in the number of pores per unit surface area at the expense of crystallite size D [21]. The crystallite size D, the average lattice parameter a, and the X-ray density D_x as determined from the powder XRD data of the recorded patterns of the compound are listed in Table I.

TABLE I. The crystallite size D (nm), average lattice parameter a (Å) and X-ray density D_x (g/cm^3) versus Co^{2+} concentration in $Co_xNi_{1-x}Mn_{0.5}Fe_{1.5}O_4$ spinel ferrites.

S.No	Co^{2+} concentration (x)	D (nm)	a (Å)	D_x (g/cm^3)
1	0	42.16	8.215	5.623
2	0.25	36.68	8.248	5.551
3	0.50	31.47	8.290	5.468
4	0.75	30.30	8.327	5.392
5	1	28.42	8.339	5.372

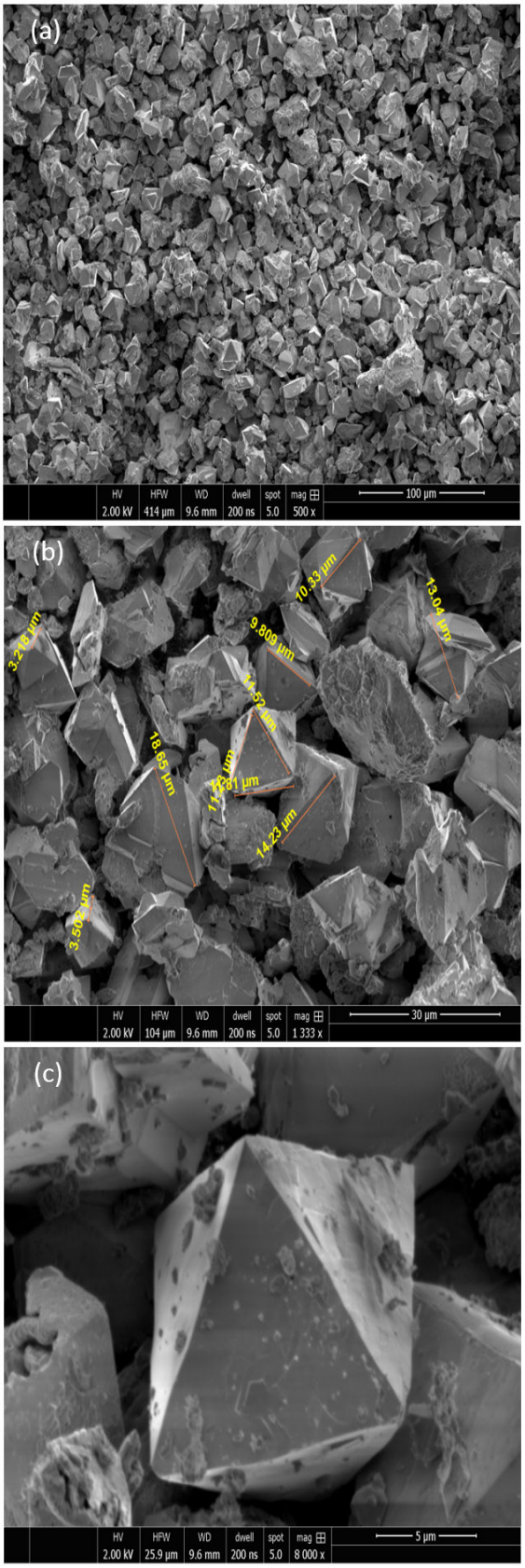

FIGURE 4. SEM micrographs of nanostructured $NiMn_{0.5}Fe_{1.5}O_4$ spinel ferrites with a) 100 μm scale, b) 30 μm scale, c) 5 μm scale.

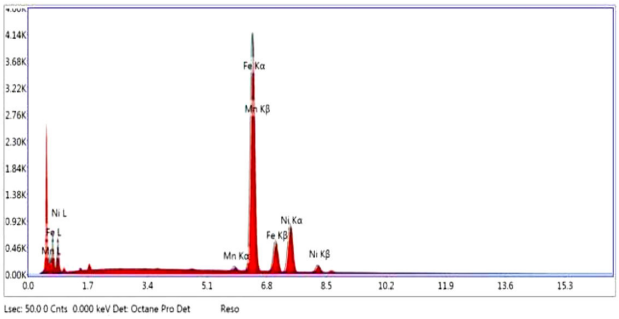

FIGURE 5. EDX spectrum of $NiMn_{0.5}Fe_{1.5}O_4$ spinel ferrite.

3.2. SEM analysis

A characteristic SEM micrograph of nanostructured $NiMn_{0.5}Fe_{1.5}O_4$ compound annealed at 600°C for 1 h is shown in Fig. 4a). The micrograph revealed the formation of almost octahedral-shaped grains as agglomerates of fine magnetic particles with sizes of the order of several microns [22-25]. The size of the grains of a compound $NiMn_{0.5}Fe_{1.5}O_4$ under investigation was estimated from the SEM micrograph shown in Fig. 4b). It was revealed that the grain size widely ranged from 3-15 μm. The diverse size distribution of grains was attributed to a varying size-dependent chaining tendency of the nanostructured ferrite particles, which constituted the grains by a huge collection of fine magnetic particles [26]. The morphological shape of the grains of $NiMn_{0.5}Fe_{1.5}O_4$ compound was studied from the SEM micrograph shown in Fig. 4c). The micrograph clearly depicted an overwhelming trend of the octahedral-shaped morphology of the grains comprising fine magnetic ferrite particles [27]. A representative EDX spectrum recorded for the $NiMn_{0.5}Fe_{1.5}O_4$ spinel ferrite composition is shown in Fig. 5. The main objective of EDX characterization was to endorse the purity and surety of the proposed chemical composition of the spinel compounds. On the investigation of the recorded spectrum, it was found that all the three kinds of cations Ni, Mn, and Fe, involved in constituting the ferrite composition under investigation were detected appropriately as the major constituent elements along with a representative peak for oxygen anions. The EDX spectrum also indicated an absence of any kind of impurity elements in the compound. Additionally, the EDX pattern reflected a good crystallinity in the nanostructured spinel ferrite compound, besides revealing that the chemical precursors had entirely undergone a chemical reaction to yield the ferrite compound [28].

3.3. TEM analysis

As the particle size of a nanostructured compound is a rational measure of the diameter of the constituent particles offering conclusive remarks on key features necessary to define a domain of the characteristics of the compound. A TEM micrograph merely offers a very first choice to exactly evaluate the particle size of a nanostructured compound under investigation. Moreover, a TEM micrograph also gives an account of the ranges of size distribution, uniformity of dispersion by perceiving the agglomeration tendency of fine particles along with the supplementary morphological details. In literature, the nanostructured spinel compounds are usually found displaying cubic, spherical, octahedral, or star-like symmetric shapes [29,30]. Herein, the TEM investigations were carried out to study the microstructure and morphology of the nanostructured $NiMn_{0.5}Fe_{1.5}O_4$ compound. Figure 6a) shows the TEM micrograph of calcined $NiMn_{0.5}Fe_{1.5}O_4$ ferrite powder. The micrograph revealed no specific morphology of the nanostructured particles reflecting a poor crystallinity and an overwhelming chaining tendency of the particles, which resulted in the formation of huge agglomerates of nanoparti-

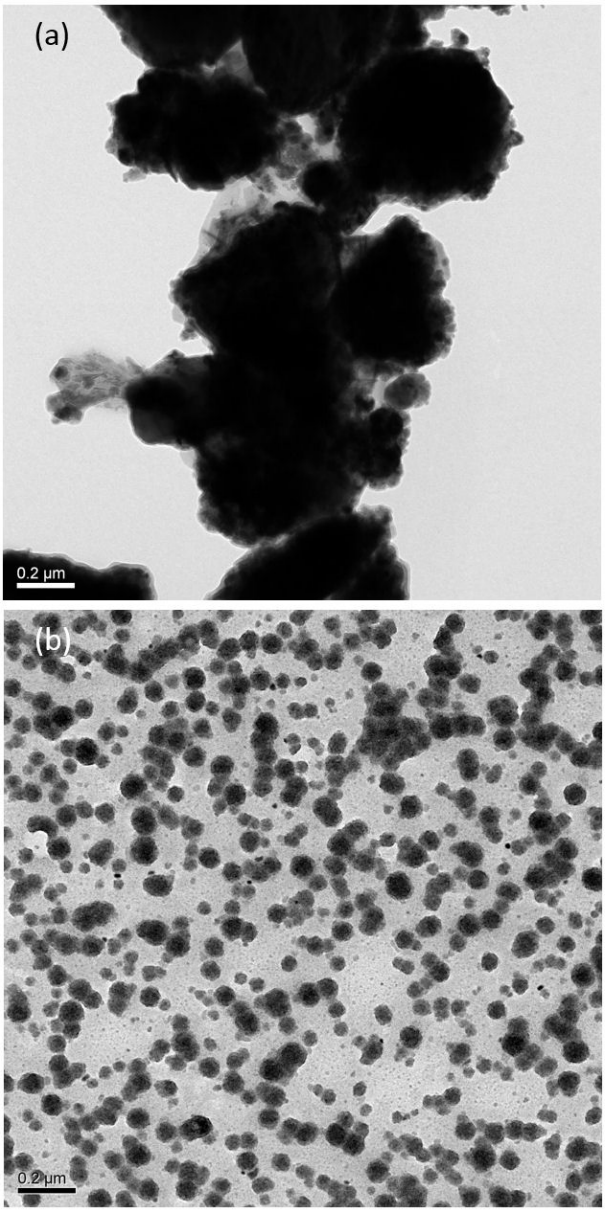

FIGURE 6. Bright field TEM micrograph of $NiMn_{0.5}Fe_{1.5}O_4$ spinel ferrite a) calcined at 120°C for 2 h b) calcined at 120°C for 2 h and annealed at 600°C for 1 h.

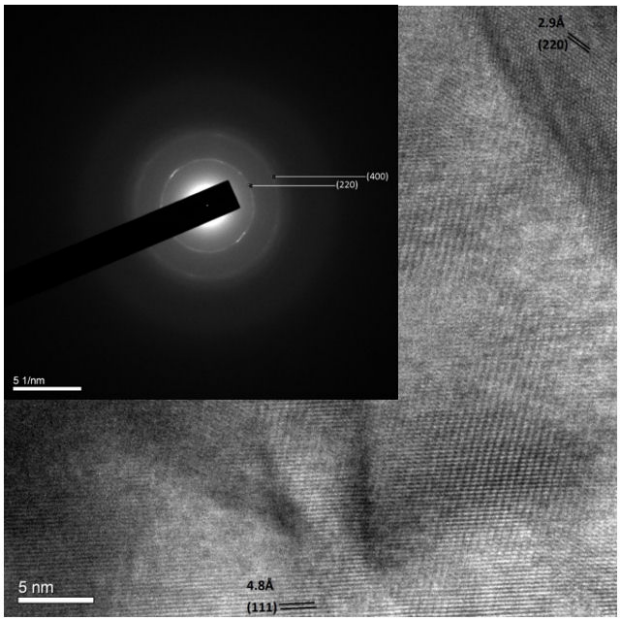

FIGURE 7. HRTEM micrograph of $NiMn_{0.5}Fe_{1.5}O_4$ spinel ferrite, inset shows the corresponding SAED pattern.

cles. Figure 6b) represents a TEM micrograph for the annealed nanostructured $NiMn_{0.5}Fe_{1.5}O_4$ ferrite compound. An investigation of the recorded micrograph revealed that the compound particles were monodispersed with nanoscale sizes possessing a closer size distribution with a display of an almost homogeneous spherical morphology. These features led to a conclusion that there was a controlled evolution of particle sizes and shape morphology of the nanostructured ferrite compounds. From the micrograph, it was also learned that the size of the particles of nanostructured $NiMn_{0.5}Fe_{1.5}O_4$ compound ranged from 20-50 nm, which was in good agreement with the size of crystallites as determined from the corresponding XRD data employing Debye-Scherer's formula [31,32]. A high-resolution TEM (HRTEM) micrograph interprets the microstructure of nanoparticles under investigation and facilitates an inspection of the thickness of crystal defects, surface orders, and polydispersity. Figure 7 shows the HRTEM micrograph of nanostructured $NiMn_{0.5}Fe_{1.5}O_4$ compound. The micrograph revealed an ordered pattern of diffraction fringes of the spinel lattice, and the fringe separations were noted to be 4.8 and 2.9 Å which corresponded to the reflection planes (111) and (220) of the standard diffraction pattern of $NiFe_2O_4$ (PDF#74-2081), respectively [26]. An inset in Fig. 7 shows the selected area electron diffraction (SAED) pattern of the nanostructured $NiMn_{0.5}Fe_{1.5}O_4$ compound. The SAED pattern involved two distinctly spotted diffraction rings indicating a polycrystalline nature of the ferrite compound under investigation. A spotted appearance of the diffraction rings in the SAED pattern was attributed to the good crystallinity of the obtained compound, and the diffraction rings were indexed to (220) and (400) reflection planes of the standard diffraction pattern of $NiFe_2O_4$ (PDF#74-2081) [27,33].

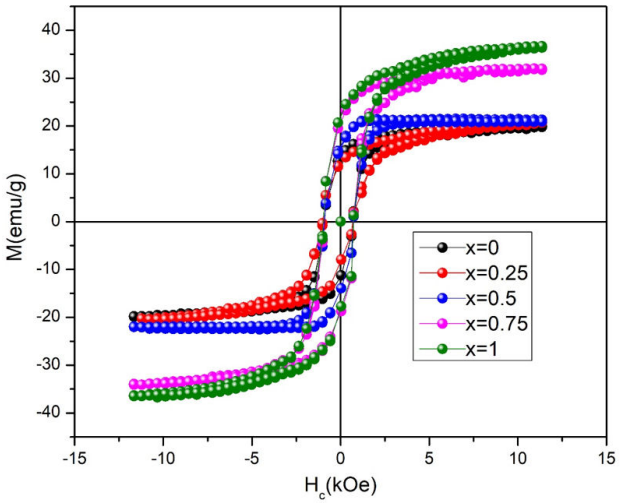

FIGURE 8. M-H hysteresis loops of $Co_xNi_{1-x}Mn_{0.5}Fe_{1.5}O_4 (x = 0, 0.25, 0.5, 0.75, 1)$ spinel ferrites.

3.4. VSM analysis

The magnetic measurements of a nanostructured ferrite compound solely depend on the chemical composition, crystalline structure, particle size distribution and morphology (34). A set of M-H hysteresis loops of the nanostructured compounds $Co_xNi_{1-x}Mn_{0.5}Fe_{1.5}O_4$ is shown in Fig. 8(a, b, c, d, e) for $Co_{1-x}Ni_xMn_{0.5}Fe_{1.5}O_4$ compounds with $x = 0$, $x = 0.25$, $x = 0.5$, $x = 0.75$ and $x = 1$, respectively. Several magnetic parameters deduced from the recorded M-H hysteresis loops are listed in Table II.

In ferrimagnetic materials like spinel ferrites which follow the Neel's two-sublattice model, there can be three types of exchange interactions among the cations distributed in tetrahedral (A-type) and octahedral (B-type) sublattices represented by A-A, A-B, and B-B interactions. The strength of the A-B interaction is greater than the rest of the two A-A and B-B interactions, and the net magnetic moment for a spinel compound is taken as M=MB-MA. A larger value of M results in a higher saturation magnetization, Ms of the spinel compound [35,36]. In the series of recorded M-H hysteresis loops, it was noted that the $NiMn_{0.5}Fe_{1.5}O_4$ ferrite ($x = 0$) showed a maximum magnetization, M_{max} of 19.98 emu/g, and on the substitution of Co^{2+} into the next successive com-

TABLA II. The coercivity H_c, maximum magnetization M_{max} and remanent magnetization M_r versus Co^{2+} concentration in $Co_xNi_{1-x}Mn_{0.5}Fe_{1.5}O_4$ spinel ferrites.

Sr.No.	Co^{2+} concentration (x)	H_c (kOe)	M_{max} (emu/g)	M_r (emu/g)
1	0	0.67	19.98	12.88
2	0.25	0.68	20.97	12.32
3	0.50	0.70	21.34	15.9
4	0.75	0.72	31.98	20.22
5	1	0.75	36.86	22.30

position ($x = 0.25$), the maximum magnetization, M_{max} experienced a slight rise (20.97 emu/g). This rise in Mmax was attributed to the cation concentration at B-site, which influenced the exchange interactions between A and B-site cations and positively led to a higher maximum magnetization, M_{max}, and thereafter, it kept the trend steadily on further increased Co^{2+} concentrations. In intermediate compositions ($x = 0.25, 0.5,$) of $Co_xNi_{1-x}Mn_{0.5}Fe_{1.5}O_4$($x = 0, 0.25, 0.5, 0.75, 1$) mixed spinel compounds, such a dependent response of Mmax was ascribed to the higher magnetic moment of Co^{2+} besides its dominating occupational affinity of the octahedral site in comparison with Ni^{2+} in the spinel lattice. A dominant substitution of Co^{2+} cations in replacement of the host Ni^{2+} cations in spinel compounds ($x = 0.75, 1$) caused a change in structure type from a mixed spinel to an inverse spinel, and hence an evident rise in magnetization was noted [37]. Due to a stable valance state and ionic size, the Mn^{3+} cation is intended to occupy the tetrahedral interstitial site. A compound with maximum Co^{2+} concentration ($x = 1$) exhibited a maximum coercivity of 0.75 kOe, which reflected that the entire series of ferrite compounds could easily be magnetized without a considerable loss of magnetic flux, and hence the ferrite compounds preserved a character of soft magnets. A significant variation in the shape of hysteresis loops on changing concentration of Co^{2+} cations enabled the ferrite compounds to be effectively applied in magnetic storage devices, microwave appliances, transformer cores, and magnetic field sensors. The series of ferrite compounds under investigation exhibited a significant soft magnetic character devised by enhanced exchange interactions among the nanostructured particles based on a larger surface to volume ratio, which in turn induced the mechanisms of spin canting, magneto-crystalline anisotropy, and super-exchange interaction [38]. An increase in Co^{2+} concentration in ferrite compounds caused a reduction in particle size at the nanoscale, boosting the surface area intact among ferrite particles. Subsequently, a quantum confinement effect in the nanostructured ferrites led to a superior magnetic character [39]. It was concluded that the interplay of the three aforementioned major interactions, *i.e.*, spin canting, superexchange interaction and magneto-crystalline anisotropy prevailed in the nanostructured compounds and the magnetic behavior of the ferrites was an outcome of the said interactions. The values of the magnetic parameters were found consistent with those reported earlier for the same family of nanostructured ferrites [40,41].

4. Conclusions

A series of nanostructured $Co_xNi_{1-x}Mn_{0.5}Fe_{1.5}O_4$($x = 0, 0.25, 0.5, 0.75, 1$) spinel ferrites was successfully synthesized by low temperature processing using sol-gel autocombustion technique which involved a shorter post-growth annealing of 1 h at lower temperature of 600°C. The XRD patterns of the ferrite compounds confirmed the formation of pure single-phase spinels, and indexing of the patterns led to an fcc structure of ferrites belonging to the Fd-$\bar{3}$m space group. Debye-Scherrer's formula endorsed the nanoscaled crystallites size of the obtained ferrites. The average lattice parameter a crystallite size D and X-ray density D_x showed a variation as a function of Co^{2+} concentration in the series of the ferrite compounds. The SEM micrographs of the $NiMn_{0.5}Fe_{1.5}O_4$ compound revealed the existence of microns-sized grains of the magnetic fine particles, which displayed an octahedral-shaped morphology. The EDX spectrum of the $NiMn_{0.5}Fe_{1.5}O_4$ferrite compound confirmed its elemental composition endorsing the completion of a proposed chemical reaction. Moreover, no impurity element was detected in the EDX spectrum of the compound. The TEM investigations of $NiMn_{0.5}Fe_{1.5}O_4$ compound revealed the particle size in nano regime consistent with the estimation of crystallite size by XRD data. An investigation of the HRTEM fringe pattern and SAED rings of $NiMn_{0.5}Fe_{1.5}O_4$ compound led to the Miller indices of the diffraction planes belonging to the standard diffraction pattern of $NiFe_2O_4$ compound. A measurement of M-H hysteresis loops of $Co_xNi_{1-x}Mn_{0.5}Fe_{1.5}O_4$($x = 0, 0.25, 0.5, 0.75, 1$) spinel ferrites revealed that the coercivity Hc, maximum magnetization Mmax and remanent magnetization Mr were strongly dependent on Co^{2+}concentration in ferrite compounds. A compound with maximum Co^{2+} concentration ($x = 1$) exhibited a superior magnetic behavior in the series of ferrite compounds.

1. J. L. O. Quiñonez, U. Pal, M. S. Villanueva, Structural, Magnetic, and Catalytic Evaluation of Spinel Co, Ni, and Co-Ni Ferrite Nanoparticles Fabricated by Low-Temperature Solution Combustion Process. *ACS Omega* **3** (2018) 14986; https://doi.org/10.1021/acsomega.8b02229.

2. C. Dong, G. Wang, D. Guo, C. Jiang, D. Xue, Growth, structure, morphology, and magnetic properties of Ni ferrite films. *Nanoscale Research Letters* **8** (2013) 196. https://doi.org/10.1186/1556-276X-8-196.

3. D. S. Mathew, R.-S. Juang, An overview of the structure and magnetism of spinel ferrite nanoparticles and their synthesis in microemulsions. *Chemical Engineering Journal* **129** (2007) 51. https://doi.org/10.1016/j.cej.2006.11.001.

4. V. Mameli, M. S. Angotzi, C. Cara, C. Cannas, Liquid Phase Synthesis of Nanostructured Spinel Ferrites — *A Review. Journal of Nanoscience and Nanotechnology* **19** (2019) 4857. https://doi.org/10.1166/jnn.2019.16808.

5. R. Srivastava, B. Yadav, Ferrite Materials: Introduction, Synthesis Techniques, and Applications as Sensors. *International Journal of Green Nanotechnology* **4** (2012), 141. https://doi.org/10.1080/19430892.2012.676918.
6. V. R. Bhagwat, A. V. Humbe, S. D. More, K. M. Jadhav, Sol-gel auto combustion synthesis and characterizations of cobalt ferrite nanoparticles: Different fuels approach. *Materials Science and Engineering: B* **248** (2019) 114388. https://doi.org/10.1016/j.mseb.2019.114388.
7. S. E. Shirsath, D. Wang, S. S. Jadhav, M. L. Mane, S. Li, *Handbook of Sol-Gel Science and Technology*, 1st Ed. (Springer International Publishing, Cham, 2017), pp. 1-41. https://doi.org/10.1007/978-3-319-19454-7_125-1.
8. I. T K, P. Lakshmi, Magnetic Nanoparticles - A Review. *Int. J. Pharm. Sci. Nanotechnol* **3** (2010) 1035. https://doi.org/10.37285/ijpsn.
9. P. Kumar, P. Mishra, S. Sahu, *Synthesis of Ni-Zn Ferrites Using Low Temperature Sol-Gel Process* (2011).
10. I. Starko, T. Tatarchuk, M. Bououdina, La-doped Ni 0.5 Co 0.5 Fe 2 O 4 nanoparticles: effect of cobalt precursors on structure and morphology. *Molecular Crystals and Liquid Crystals* **674** (2018) 110. https://doi.org/10.1080/15421406.2019.1578517.
11. N. G. Deshpande, C. H. Ahn, D. S. Kim, S. H. Jung, Y. B. Kim, H. K. Cho, Bifunctional reusable Co0.5Ni0.5Fe2O4 nanoparticle-grafted carbon nanotubes for aqueous dye removal from contaminated water. *Catalysis Science & Technology*. **10** (2020) 6188. https://doi.org/10.1039/D0CY01057J.
12. D. M. Coutinho, V. M. S. Verenkar, Preparation, spectroscopic and thermal analysis of hexa-hydrazine nickel cobalt ferrous succinate precursor and study of solid-state properties of its nanosized thermal product, Ni0.5Co0.5Fe2O4. *Journal of Thermal Analysis and Calorimetry* **128** (2017) 807. https://doi.org/10.1007/s10973-016-6011-8.
13. A. V. Humbe, J. S. Kounsalye, S. B. Somvanshi, A. Kumar, K. M. Jadhav, Cation distribution, magnetic and hyperfine interaction studies of Ni-Zn spinel ferrites: role of Jahn Teller ion (Cu2+) substitution. *Materials Advances* 1 (2020) 880. https://doi.org/10.1039/D0MA00251H.
14. W. Agami, M. Ashmawy, Structural, physical, and magnetic properties of nanocrystalline manganese-substituted lithium ferrite synthesized by sol-gel autocombustion technique. *Applied Physics A* **126** (2020) 563. https://doi.org/10.1007/s00339-020-03737-6.
15. K. V. Babu, G. Satyanarayana, B. Sailaja, G. V. S. Kumar, K. Jalaiah, M. Ravi, Structural and magnetic properties of Ni0.8M0.2Fe2O4 (M=Cu, Co) nano-crystalline ferrites. *Results in Physics* **9** (2018) 55. https://doi.org/10.1016/j.rinp.2018.01.048.
16. K. V. Babu, B. Sailaja, K. Jalaiah,T. P. Shibeshi, M. Ravi, Effect of zinc substitution on the structural, electrical and magnetic properties of nano-structured Ni0.5Co0.5Fe2O4 ferrites. *Physica B Condensed Matter* **534** (2018) 83. https://doi.org/10.1016/j.physb.2018.01.022.
17. M. K. Kokare, N. A. Jadhav, Y. Kumar, K. M. Jadhav, S. M. Rathod, Effect of Nd3+ doping on structural and magnetic properties of Ni0.5Co0.5Fe2O4 nanocrystalline ferrites synthesized by sol-gel auto combustion method. *Journal of Alloys and Compounds* **748** (2018) 1053. https://doi.org/10.1016/j.jallcom.2018.03.168.
18. W. Liu, G. Tan, G. Dong, H. Ren, A. Xia, Influence of multi-ion co-doping and NiFe2O4 layer on the properties of BiFeO3/NiFe2O4 composite films by sol-gel. *Materials Letters* **142** (2015) 27-29. https://doi.org/10.1016/j.matlet.2014.11.141.
19. H. Saqib, S. Rahman, R. Susilo, B. Chen, N. Dai, Structural, vibrational, electrical, and magnetic properties of mixed spinel ferrites $Mg_{1-x}Zn_xFe_2O_4$ nanoparticles prepared by co-precipitation. *AIP Advances* **9** (2019) 055306. https://doi.org/10.1063/1.5093221.
20. H. Shokrollahi, L. Avazpour, Influence of intrinsic parameters on the particle size of magnetic spinel nanoparticles synthesized by wet chemical methods. *Particuology* **26** (2016) 32. https://doi.org/10.1016/j.partic.2015.10.004.
21. P. Thakur, A. Thakur, M. Singh, *Effect of particle size on the properties of Mn-Zn-In ferrites.* **77** (2008) 25701. https://doi.org/10.1088/0031-8949/77/02/025701.
22. G. Padmapriya, A. Manikandan, V. Krishnasamy, S. K. Jaganathan, S. A. Antony, Spinel $N_{ix}Zn_{1-x}Fe_2O_4$ ($0.0 \leq x \leq 1.0$) nano-photocatalysts: Synthesis, characterization and photocatalytic degradation of methylene blue dye. *Journal of Molecular Structure* **1119** (2016) 39. https://doi.org/10.1016/j.molstruc.2016.04.049.
23. L. Zheng, K. Fang, M. Zhang, Z. Nan, L. Zhao, D. Zhou, M. Zhu, W. Li, Tuning of spinel magnesium ferrite nanoparticles with enhanced magnetic properties. *RSC Advances* **8** (2018) 39177. https://doi.org/10.1039/C8RA07487A.
24. N. Deraz, A. Alarifi, Synthesis and Physicochemical Properties of Nanomagnetic Zinc Ferrite System. International Journal of Electrochemical Science **7** (2012) 3798.
25. W. Wang, Z. Ding, X. Zhao, S. Wu, F. Li, M. Yue, J. P. Liu, Microstructure and magnetic properties of MFe_2O_4 (M = Co, Ni, and Mn) ferrite nanocrystals prepared using colloid mill and hydrothermal method. *Journal of Applied Physics* **117** (2015) 17A328. https://doi.org/10.1063/1.4917463.
26. Z. Xu, J. Fan, T. Liu, Y. Han, H. Zhang, Calcination induced phase transformation in MnZn ferrite powders. *Journal of Alloys and Compounds* **814** (2020) 152307. https://doi.org/10.1016/j.jallcom.2019.152307.
27. Z. Xu, J. Fan, Y. Han, T. Liu, H. Zhang, K. Song, C. Zhang, Preparation and characterization of Mn-Zn ferrites via nano-in-situ composite method. *Solid State Sciences* **98** (2019) 106006. https://doi.org/10.1016/j.solidstatesciences.2019.106006.
28. T. Tatarchuk, M. Bououdina, W. Macyk, O. Shyichuk, N. Paliychuk, I. Yaremiy, B. Al-Najar, M. Pacia, Structural, Optical, and Magnetic Properties of Zn-Doped CoFe(2)O(4) Nanoparticles. *Nanoscale research letters* **12** (2017) 141. https://doi.org/10.1186/s11671-017-1899-x.
29. M. Lakshmi, K. Vijaya Kumar, K. Thyagarajan, An investigation of structural and magnetic properties of Cr-Zn ferrite nanoparticles prepared by a sol-gel process. *Journal of Nanostructure in Chemistry* **5** (2015) 365. https://doi.org/10.1007/s40097-015-0168-8.

30. L. T. Lu, N. T. Dung, L. D. Tung, C. T. Thanh, O. K. Quy, N. V. Chuc, S. Maenosono, N. T. K. Thanh, Synthesis of magnetic cobalt ferrite nanoparticles with controlled morphology, monodispersity and composition: the influence of solvent, surfactant, reductant and synthetic conditions. *Nanoscale* **7** (2015) 19596. https://doi.org/10.1039/C5NR04266F.

31. T. Petrova, N. Velinov, D. Filkova, I. Ivanova, I. Ivanov, I. Yordanova, S. Todorova, V. Idakiev, N. Petrov, I. Mitov, Synthesis and characterization of supported spinel ferrite catalysts. *Journal of Chemical Technology and Metallurgy* **53** (2018) 1186.

32. S. Modak, M. Ammar, F. Mazaleyrat, S. Das, P. K. Chakrabarti, XRD, HRTEM and magnetic properties of mixed spinel nanocrystalline Ni-Zn-Cu-ferrite. *Journal of Alloys and Compounds* **473** (2009) 15. https://doi.org/10.1016/j.jallcom.2008.06.020.

33. D. R. Kumar, S. I. Ahmad, C. A. Lincoln, D. Ravinder, Structural, optical, room-temperature and low-temperature magnetic properties of Mg-Zn nanoferrite ceramics. *Journal of Asian Ceramic Societies* **7** (2019) 53. https://doi.org/10.1080/21870764.2018.1563036.

34. R. S. Pandav, R. P. Patil, S. S. Chavan, I. S. Mulla, P. P. Hankare, Magneto-structural studies of sol-gel synthesized nanocrystalline manganese substituted nickel ferrites. *Journal of Magnetism and Magnetic Materials* **417** (2016) 407. https://doi.org/10.1016/j.jmmm.2016.04.090.

35. M. A. Rafiq, A. Javed, M. N. Rasul, M. A. Khan, A. Hussain, Understanding the structural, electronic, magnetic and optical properties of spinel MFe_2O_4 (M=Mn, Co, Ni) ferrites. *Ceramics International* **46** (2020) 4976. https://doi.org/10.1016/j.ceramint.2019.10.237.

36. A. Hussain, T. Abbas, S. Niazi, Preparation of $Ni_{1-x}Mn_xFe_2O_4$ ferrites by sol-gel method and study of their cation distribution. *Ceramics International* **39** (2013) 1221. https://doi.org/10.1016/j.ceramint.2012.07.049.

37. L. C. Xue, L. L. Lang, J. Xu, Z. Z. Li, W. H. Qi, G. D. Tang, L. Q. Wu, Magnetic moment directions and distributions of cations in Cr (Co) substituted spinel ferrites $Ni_{0.7}Fe_{2.3}O_4$. *AIP Advances* **5** (2015) 097167. https://doi.org/10.1063/1.4931919.

38. F. G. da Silva, J. Depeyrot, A. Campos, R. Aquino, D. Fiorani, D. Peddis, Structural and Magnetic Properties of Spinel Ferrite Nanoparticles. *Journal of Nanoscience and Nanotechnology* **19** (2019) 1. https://doi.org/10.1166/jnn.2019.16877.

39. N. N. Mojumder, C. Augustine, D. E. Nikonov, K. Roy, Effect of quantum confinement on spin transport and magnetization dynamics in dual barrier spin transfer torque magnetic tunnel junctions. *Journal of Applied Physics* **108** (2010) 104306. https://doi.org/10.1063/1.3503882.

40. U. Salazar-Kuri, J. O. Estevez, N. R. Silva-González, U. Pal, M. E. Mendoza, Structure and magnetic properties of the $Co_{1-x}Ni_xFe_2O_4$-$BaTiO_3$ core-shell nanoparticles. *Journal of Magnetism and Magnetic Materials* **442** (2017) 247. https://doi.org/10.1016/j.jmmm.2017.06.126.

41. H. Y. He, Structural and Magnetic Property of $Co_{1-x}Ni_xFe_2O_4$ Nanoparticles Synthesized by Hydrothermal Method. *International Journal of Applied Ceramic Technology* **11** (2014) 626. https://doi.org/10.1111/ijac.12071.